Supramolecular Chemistry

International Edition: DOI: 10.1002/anie.201602713
German Edition: DOI: 10.1002/ange.201602713

Regio-, Stereo-, and Atropselective Synthesis of C_{60} Fullerene Bisadducts by Supramolecular-Directed Functionalization

Giovanni Bottari, Olga Trukhina, Axel Kahnt, Michael Frunzi, Yasujiro Murata, Antonio Rodríguez-Fortea, Josep M. Poblet, Dirk M. Guldi,* and Tomás Torres**

Dedicated to Professor Luis Echegoyen on the occasion of his 65th birthday

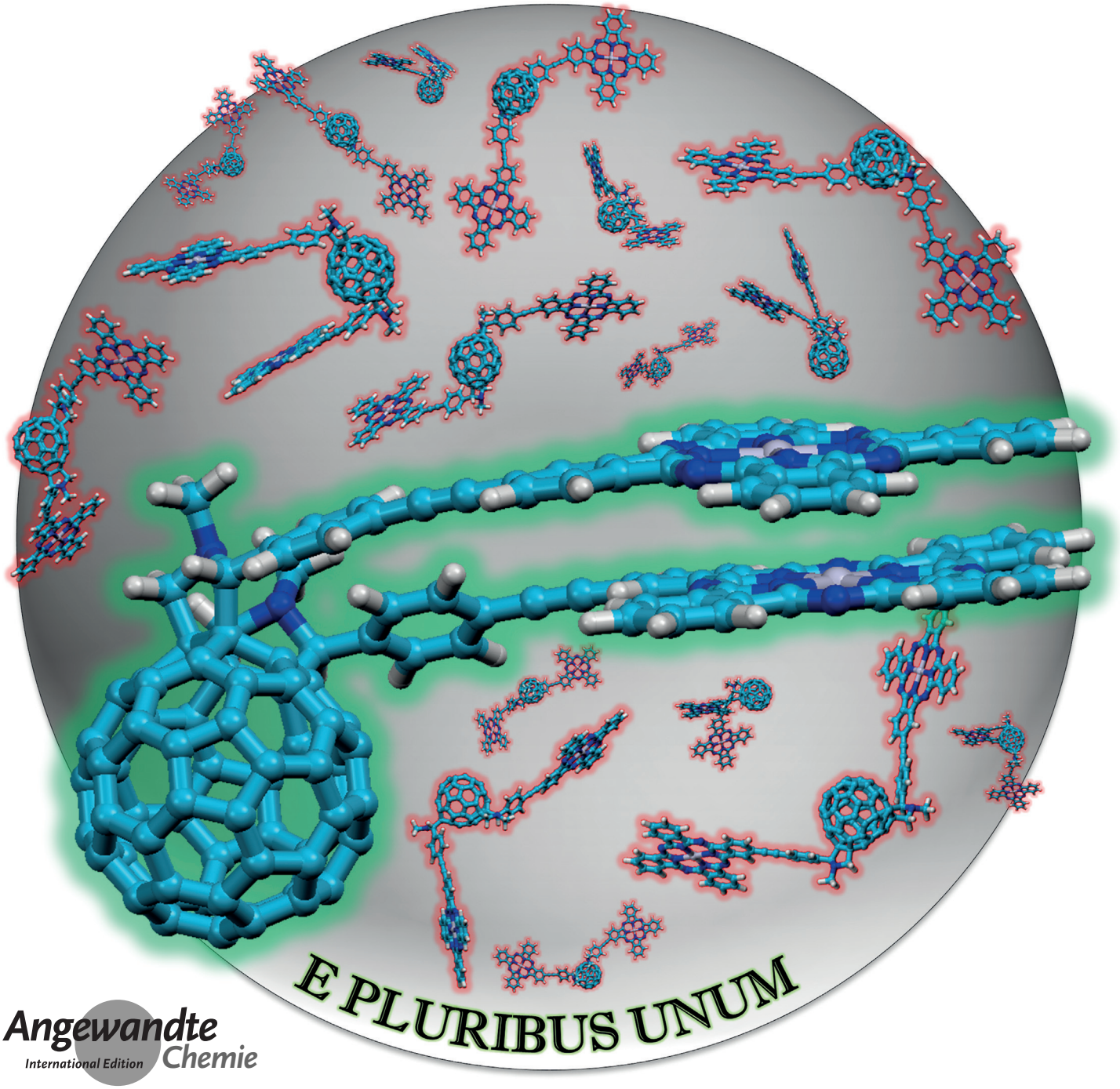

Angewandte International Edition Chemie

Abstract: *The regio- and stereocontrolled synthesis of fullerene bisadducts is a topic of increasing interest in fullerene chemistry and a key point for the full exploitation of these derivatives in materials science. In this context, while the tether-directed remote functionalization strategy offers a valid approach to this synthetic challenge, no examples of such control have yet been reported using nontethered species. Presented here is a conceptually novel, supramolecular-directed functionalization approach in which noncovalent interactions between untethered residues have been used, for the first time, to amplify (>2800-fold) the regio-, stereo-, and atropselective formation of a C_{60} fullerene bisadduct racemate from a complex mixture of 130 bisadducts. Remarkably, both enantiomers, which present a sterically demanding cis-1 C_{60} addition pattern, represent the first examples of fullerene derivatives which combine central, axial, and helical chirality.*

During the last decade, the preparation and study of fullerene bisadducts has gained increasing interest in the field of fullerene chemistry and organic photovoltaics.[1–6] An important issue related to the preparation of such derivatives is how to promote their regio- and, in some cases, stereocontrolled synthesis, which is not a trivial task considering that fullerenes present several double bonds (e.g., 30 in the case of C_{60}) distributed over their spherical structure and all of them have either identical or similar reactivity. In one of the simplest cases, such as the cycloaddition to C_{60} of two highly symmetrical and nonprochiral chemical species, a maximum of eight C_{60} bisadduct regioisomers could theoretically form based on the eight C_{60} addition patterns (see Figure S5.1a in the Supporting Information).[7] However, the isolation of these bisadducts is often difficult, and necessarily involves the use of tedious purification protocols.

An important step towards the controlled synthesis of C_{60} bisadducts has been made possible by the use of the tether-directed remote functionalization introduced by Diederich and co-workers.[8] This synthetic methodology consists of covalently linking the two residues, which will ultimately add to C_{60}, by a spacer having structural and conformational features that lead to the preferred formation of certain C_{60} bisadducts.[9] This strategy, used almost exclusively in cyclopropanation reactions, has been successfully employed for the preparation of C_{60} bisadducts with excellent regioselectivity[10–14] and, in some cases, good stereoselectivity.[15–17] By using this methodology, sterically demanding *cis*-1 C_{60} bisadducts have also been obtained.[18–20]

Significantly more difficult, and to the best of our knowledge unprecedented, is the possibility to carry out a controlled synthesis of C_{60} bisadducts using untethered and prochiral (or low-symmetry) residues. In this case, a large number of C_{60} bisadducts could be formed with no regio- and stereocontrol because of the lack of any bias for guiding the cycloaddition of the two residues to specific positions of the C_{60} cage. For example, in the case of the 1,3-dipolar cycloaddition reaction of untethered, prochiral azomethine ylides to C_{60} fullerene, one of the most straightforward C_{60} functionalization methods[21] and the reaction employed in this work, up to 130 C_{60} bisadducts having different regio- and stereochemistry could theoretically form (see Section 5 in the Supporting Information).

In this work, we present a supramolecular-directed functionalization approach which has been used, for the first time, to promote the regio-, stereo-, and atropselective synthesis of untethered C_{60} bisadducts. This strategy takes advantage of noncovalent interactions between untethered phthalocyanine (Pc) species to boost (>2800-fold) the formation of a pair of Pc_2–C_{60} bisadduct enantiomers for which the structure was determined by a combination of experimental techniques and theoretical calculations. Remarkably, and to our surprise, such an untethered bisaddition reaction not only proceeds with excellent regio- and stereoselectivity furnishing two enantiomers which present a *cis*-1 C_{60} addition pattern, but it is also highly atropselective as a result of the restricted rotation of the two Pc macrocycles in the products, thus representing the first example of an atropselective reaction in fullerene chemistry.

The synthesis of the Pc_2–C_{60} bisadducts *M*/*P*-**1**(S_a,R_a) (Figure 1), obtained as a racemic mixture of the *M*-**1**(S_a,R_a) and *P*-**1**(S_a,R_a) enantiomers, involves the reaction of Zn^{II}Pc aldehyde **2**, which was used as a mixture of regioisomers (see Figure S2.13), with C_{60} fullerene in the presence of *N*-methyl glycine in refluxing toluene (thereafter referred to as the standard reaction). From this reaction, three main products were isolated by silica gel column chromatography (see Figure S2.1a) and identified by matrix-assisted laser desorption/ionization-time of flight mass spectrometry (MALDI-MS) as the Pc–C_{60} monoadduct **3**[22] and Pc_2–C_{60} bisadducts *M*/*P*-**1**(S_a,R_a) and **4**, which were obtained in 29, 14, and 23% yield, respectively (Figure 1; see Figures S2.8, S2.4, S2.11).

The UV/Vis absorption features of *M*/*P*-**1**(S_a,R_a), **3**, and **4**, and starting material **2** in THF were then investigated (Figure 2a). In the case of **3** and **4**, the similarity between

[*] Dr. G. Bottari, Dr. O. Trukhina, Prof. Dr. T. Torres
Departamento de Química Orgánica, Universidad Autónoma de Madrid, Campus de Cantoblanco, 28049 Madrid (Spain)
and
IMDEA-Nanociencia, Campus de Cantoblanco, 28049 Madrid (Spain)
E-mail: giovanni.bottari@uam.es
tomas.torres@uam.es
Dr. A. Kahnt, Prof. Dr. D. M. Guldi
Department of Chemistry and Pharmacy
Interdisciplinary Center for Molecular Materials (ICMM)
Friedrich-Alexander-Universität Erlangen-Nürnberg
Egerlandstrasse 3, 91058 Erlangen (Germany)
E-mail: dirk.guldi@fau.de
Dr. A. Rodríguez-Fortea, Prof. Dr. J. M. Poblet
Departament de Química Física i Inorgànica, Universitat Rovira i Virgili, Campus Sescelades, 43007 Tarragona (Spain)
Prof. Dr. Y. Murata
Institute for Chemical Research, Kyoto University
Uji, Kyoto 611-0011 (Japan)
Dr. M. Frunzi
Department of Chemistry, Columbia University
New York, NY 10027 (USA)
Supporting information and the ORCID identification number(s) for the author(s) of this article can be found under http://dx.doi.org/10.1002/anie.201602713.

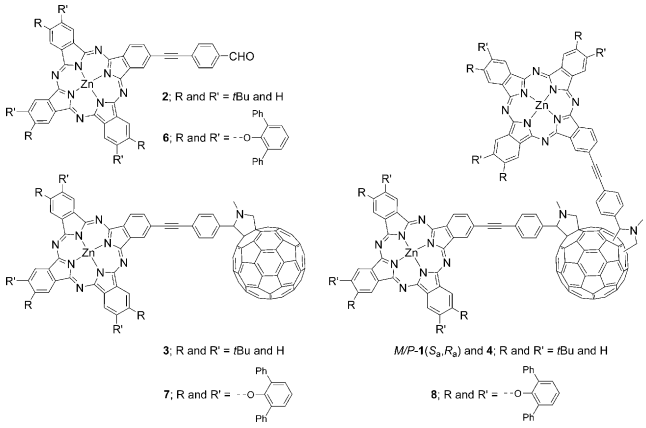

Figure 1. Molecular structures of the aldehyde-substituted Pcs **2** and **6**, and Pc-based C_{60} monoadducts **3** and **7**, and bisadducts *M*/*P*-**1**(S_a,R_a), **4**, and **8**.

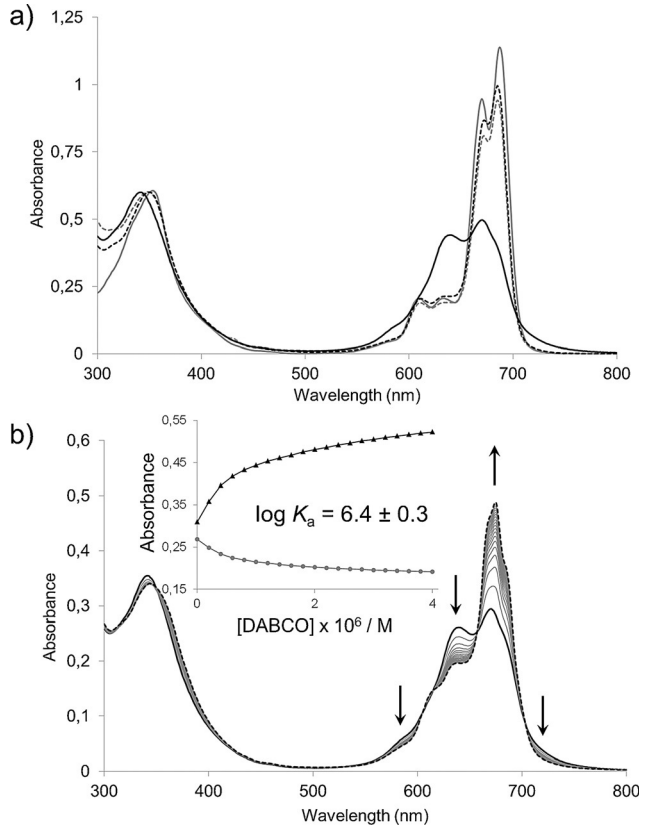

Figure 2. a) Normalized UV/Vis spectra (THF) of **2** (solid gray), **3** (dashed gray), *M*/*P*-**1**(S_a,R_a) (solid black), and **4** (dashed black). b) UV/Vis titration of *M*/*P*-**1**(S_a,R_a) (THF, 2×10^{-3} M, solid black spectrum) upon addition of DABCO (THF, 2×10^{-2} M, each addition correspond to 0.1 equiv, up to a total of 2 equiv (dashed black spectrum)). Inset: Binding isotherms at 640 (gray circles) and 670 nm (black triangles), solid lines represent the fits. DABCO = 1,4-diazabicyclo[2.2.2]octane, THF = tetrahydrofuran.

the UV/Vis spectra of these two C_{60} adducts and **2** suggests negligible ground-state electronic communication 1) between the Pc and the C_{60} moieties in the former derivatives and 2) between the two Pc macrocycles in **4**, macrocycles which behave like electronically independent moieties. In contrast, and to our surprise, the UV/Vis spectrum of *M*/*P*-**1**(S_a,R_a) was significantly different from the spectra of **2**–**4**. *M*/*P*-**1**(S_a,R_a) showed a *Q*-band having two broad and equally intense absorptions with a maximum at $\lambda = 640$ and 670 nm, both weaker than the *B*-band at $\lambda = 341$ nm (Figure 2a). Concentration-dependent UV/Vis studies on *M*/*P*-**1**(S_a,R_a) in THF did not show significant changes in the position and shape of the Pc *B*- and *Q*-bands (see Figure S2.5), thus suggesting that the observed absorptions arise from some kind of intramolecular interactions. More precisely, in the UV/Vis spectrum of *M*/*P*-**1**(S_a,R_a), the presence of an intense and blue-shifted *Q*-band transition at $\lambda = 640$ nm is a clear indication of an intramolecular *H*-type stacking arrangement of the two Pc macrocycles (see Section 4).[23]

Next, UV/Vis titration experiments were carried out on *M*/*P*-**1**(S_a,R_a) using pyridine, pyrazine, and 1,4-diazabicyclo-[2.2.2]octane (DABCO). These mono- and dinitrogenated ligands were chosen with the aim of disrupting the intramolecular interaction between the two Zn^{II}Pc units in *M*/*P*-**1**(S_a,R_a) by axial coordination of the ligand nitrogen atom at the Zn^{II}Pc metal center.[24] Additionally, UV/Vis titration experiments on **3** and **4**, using the three nitrogenated ligands, were carried out. For the two latter C_{60} adducts, minor or insignificant changes in the shape and position of the Pc absorption bands were observed upon addition of any of the three ligands (see Figures S2.9, S2.12). Similarly, addition of either pyridine or pyrazine to *M*/*P*-**1**(S_a,R_a) did not cause any change in its UV/Vis spectrum (see Figure S2.6).

In contrast, and to our surprise, different results were obtained when *M*/*P*-**1**(S_a,R_a) was titrated with DABCO, which has a N···N distance (2.6 Å) comparable to that in pyrazine (2.7 Å), but significantly higher basicity ($pK_a = 8.7$ vs. 0.5),[25] and thus better metal–ligand coordination ability. In this case, a gradual decrease in the intensity of the racemate transition at $\lambda = 640$ nm was observed upon addition of DABCO together with a simultaneous increase of the band at $\lambda = 670$ nm (Figure 2b). Well-defined isosbestic points at $\lambda = 350$, 604, 656, and 704 nm suggest the formation of the supramolecular complex DABCO⊂*M*/*P*-**1**(S_a,R_a), whose 1:1 stoichiometry was determined by Job plot analysis and mass spectrometry (see Figures S2.7a and S2.7b). Multivariable analysis of the titration spectra afforded an association constant (K_a) for DABCO⊂*M*/*P*-**1**(S_a,R_a) of $\log K_a = 6.4 \pm 0.3$ in THF and at room temperature (inset Figure 2b). Such a high K_a value suggests an excellent complementarity between the tweezer-like geometry of *M*/*P*-**1**(S_a,R_a), resulting from the *H*-type stacked arrangement adopted by the two Zn^{II}Pc units, and the guest molecule DABCO. As a consequence of the complexation of DABCO into the binding pocket of *M*/*P*-**1**(S_a,R_a), π-stacking interactions between the two Pc units are disrupted, thus giving rise to the observed changes in the *Q*-band absorption.

Next, photophysical studies on the bisadduct isomers *M*/*P*-**1**(S_a,R_a) and **4** were carried out showing important differences between them in terms of fluorescence quantum yield and photoinduced charge separated lifetimes (see Section 8.2 and Table S8.1). Interestingly, upon addition of DABCO to *M*/*P*-**1**(S_a,R_a), an increase in the fluorescence

quantum yield (from 0.003 to 0.017 in toluene; see Figure S8.2) and radical ion pair state lifetime (from 254 to 3970 ps in anisole; see Figure S8.17 and Table S8.1) of the DABCO-complexed *M*/*P*-**1**(S_a,R_a) with respect to the uncomplexed racemate was observed. These latter findings can be rationalized on the basis of a decrease of the driving force for the photoinduced electron transfer in *M*/*P*-**1**(S_a,R_a) upon DABCO complexation (see Figure S8.17). Significant differences between *M*/*P*-**1**(S_a,R_a), **3**, and **4** were also observed in cyclic voltammetry (see Figures S2.14 and S2.15), and low- (see Figures S2.3 and S2.10) and high-field ^{1}H NMR studies. In the latter case H_2@C_{60} analogues of *M*/*P*-**1**(S_a,R_a), **3**, and **4** were used (see Section 9 and Figure S9.2).

Next, theoretical calculations were used with the aim of identifying, among the possible 130 Pc_2–C_{60} bisadducts, the three-dimensional (3D) structure of the enantiomers *M*-**1**(S_a,R_a) and *P*-**1**(S_a,R_a), a piece of information impossible to obtain using exclusively spectroscopic and spectrometric techniques. To this end, molecular mechanics (MM+) was initially used (see Section 6.1) to model the 72 Pc_2–C_{60} bisadducts (only one enantiomer was calculated for each of the 58 Pc_2–C_{60} enantiomer pairs which could be theoretically obtained out of the 130 possible Pc_2–C_{60} bisadducts) and their structural complexity (each bisadduct presents more than 190 nonhydrogen atoms and two zinc metal centers). However, this search was considerably simplified because of: 1) the rigid structure of the two bisadduct subunits (i.e., Pc and C_{60} fullerene) and 2) the stiffness of the phenyl-ethynyl spacer connecting each of the two Pc units to the fulleropyrrolidine moiety (Figure 3; see Figures S6.6–S6.13). A detailed analysis of the 72 MM+-minimized bisadducts showed that only two of these structures, namely derivatives *cis*-1 (A) and *cis*-1 (P,S_a,R_a) (see Figure S6.6), could give rise to an intramolecular π-stacked, *H*-type arrangement of the two Pc moieties, whereas for the other Pc_2-C_{60} bisadducts the distance between the two Pc planes in the minimized structures was either too large and/or their relative orientation inappropriate to give rise to any intramolecular *H*-type

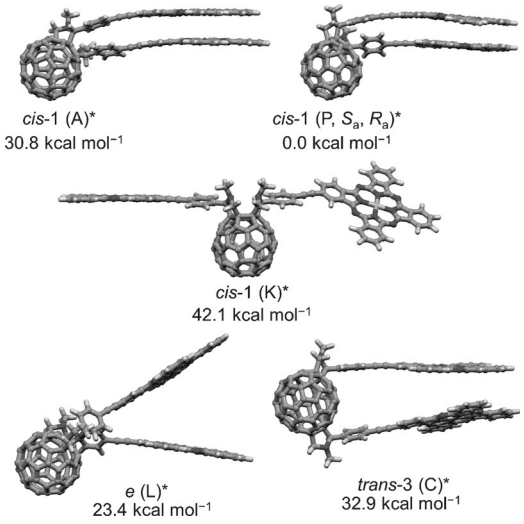

Figure 3. DFT-optimized structures of five Pc_2–C_{60} bisadducts. Below each structure, its relative energy (in kcal mol^{-1}) is reported.

aggregate. These two bisadducts were then selected, together with the reference bisadducts *cis*-1 (K), *trans*-3 (C), and *e* (L), and optimized at the DFT level with the inclusion of dispersion corrections (Figure 3; see Section 6.2 and Figure S6.16). These studies show that the *cis*-1 (P,S_a,R_a)*, an analogue of *P*-**1**(S_a,R_a), in which the six *tert*-butyl groups on the two Pc macrocycles have been replaced by six hydrogen atoms, is significantly more stable than the other four bisadducts (see Table S6.1). This large stabilization, which is surprising considering that the *cis*-1 adduct is, among the eight possible C_{60} addition patterns, the least favored because of steric reasons,[26,27] results from the favorable intramolecular Pc π-stacking interactions in *cis*-1 (P,S_a,R_a)*, and was estimated to be around 40 kcal mol^{-1}.[28] In contrast, the significant energy difference between the Pc π-stacked *cis*-1 (P,S_a,R_a)* and *cis*-1 (A)* (ca. 31 kcal mol^{-1}) essentially comes from the large steric requirement and bond distortion of the latter bisadduct with respect to *cis*-1 (P,S_a,R_a)* (see Figure S6.20).

Some important points regarding the structural features of *P*-**1**(S_a,R_a) are worth mentioning. *P*-**1**(S_a,R_a) could be erroneously considered a *meso* compound by looking exclusively at the regiochemistry of the C_{60} double addition and the configuration of its two stereogenic centers (see Figure S5.6, model P). However, it is instead a chiral molecule since it has no mirror plane and presents a right-handed (*P*) helical structure (Figure 4a; see Section 7 and Figure S7.6a). Obviously, because of the absence of any chiral bias in the reaction, the *M*-**1**(S_a,R_a) enantiomer (see Figure S2.2) is also formed together with *P*-**1**(S_a,R_a), thus leading to racemate *M*/*P*-**1**(S_a,R_a).

Moreover, it is worth noting that *M*/*P*-**1**(S_a,R_a) presents a *cis*-1 C_{60} addition pattern. The *cis*-1 C_{60} bisadducts are formed in the lowest relative yield with respect to the other C_{60} bisadducts (usually in a 1.4% relative yield in 1,3 dipolar cycloaddition reactions of untethered and non-prochiral azomethyne ylides to C_{60}),[27] mainly because of the severe steric requirements imposed by this vicinal bisaddition (see Figure S5.14). Taking this into account, and considering that 16 isomers are theoretically possible in the case of the *cis*-1 C_{60} bisaddition of two prochiral azomethyne ylides, as in this work (see Figure S5.6), a relative yield of 0.088% (i.e., a sixteenth of 1.4%) should be expected for each of the 16 *cis*-1 isomers. In the case of *M*/*P*-**1**(S_a,R_a), its relative yield would further decrease to 0.022% (i.e., a forth of 0.088%) considering that three more atropisomers, namely *M*/*P*-**1**(R_a,R_a), *M*/*P*-**1**(S_a,S_a), and *M*/*P*-**1**(R_a,S_a), could also theoretically form, each of them obtained as a racemic mixture of the *M* (Figure 4b–d; see Figure S7.6b–d) and *P* (see Figure S2.2) isomers (for a detailed account of the four Pc_2–C_{60} atropisomers and their chiral elements see Section 7). The four atropisomers have the same stereoconfiguration at their two stereogenic centers and regiochemistry but different spatial arrangement of the two Pcs because of the hindered rotation around the phenyl-ethynyl spacers. A comparison of the energetics of *P*-**1**(S_a,R_a), *P*-**1**(R_a,R_a), *P*-**1**(S_a,S_a), and *P*-**1**-(R_a,S_a), which present similar distances between their quasi-parallel Pc planes, show that the latter three atropisomers are, respectively, 7.2, 6.5, and 31.8 kcal mol^{-1} higher in energy than

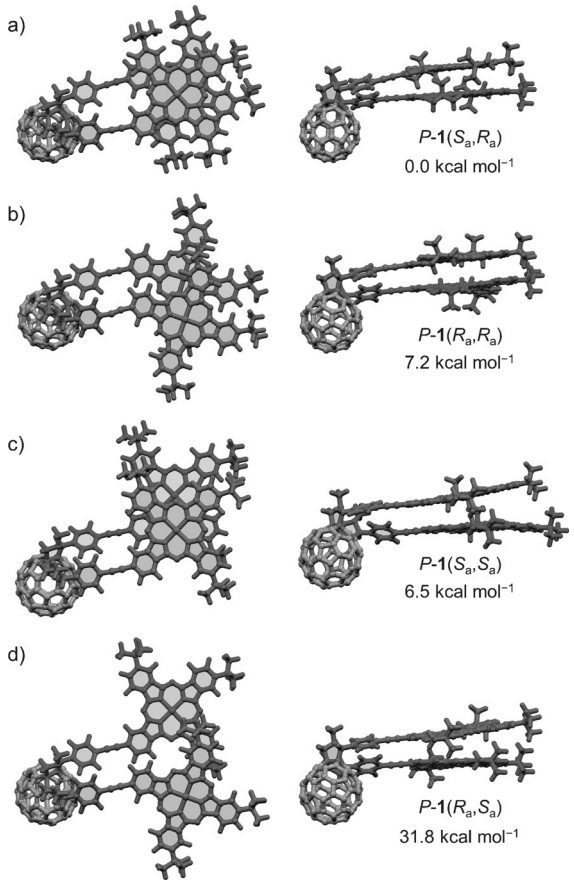

Figure 4. a–d) DFT-minimized structures (see Section 6) of *cis*-1 Pc_2–C_{60} bisadduct atropisomers a) *P*-**1**(S_a,R_a), b) *P*-**1**(R_a,R_a), c) *P*-**1**(S_a,S_a), and d) *P*-**1**(R_a,S_a). Below each DFT-minimized structure, its relative energy (in kcal mol^{-1}) is reported (see Figure S7.6).

P-**1**(S_a,R_a) (see Table S6.5). Aside from energetics considerations, the partial stacked arrangement of the two Pcs in *P*-**1**(R_a,R_a), *P*-**1**(S_a,S_a), and *P*-**1**(R_a,S_a) would not explain the remarkable complexation ability of these Pc_2–C_{60} bisadducts towards DABCO (i.e., the three atropisomers have exceedingly large Zn···Zn distances of 5.9, 5.6, and 10.7 Å, respectively, vs. 3.6 Å for the *P*-**1**(S_a,R_a) bisadduct). Moreover, the three latter atropisomers present α values (i.e., the tilt angle between the polarization axis of a Zn^{II}Pc and the line connecting the two zinc metal centers; see Sections 4 and 6.3) of about 34.6°, 36.3° and 18.2°, respectively, values which are quite far from the ones typical of *H*-aggregates (54.7° > α > 90°; α for *P*-**1**(S_a,R_a) is 74.2°) and more proper of *J*-aggregates (0° > α > 54.7°).

In this context, considering the 0.022% theoretical relative yield of *M*/*P*-**1**(S_a,R_a) and the 23% isolated yield of all Pc_2–C_{60} compounds, namely **4**, the yield of *M*/*P*-**1**(S_a,R_a) should be, at the very best, no higher than 0.005% (i.e., 0.022% of 23%). On the contrary, and to our surprise, *M*/*P*-**1**(S_a,R_a) was isolated in a 14% yield which represents a remarkable 2800-fold increase (i.e., 14/0.005) with respect to the theoretical yield (see Section 5). The true amplification is probably much higher than 2800-fold considering that the relative yield for the *cis*-1 bisaddition used for the calculations above (i.e., 1.4%) is the one obtained for unsubstituted fulleropyrrolidines and not for sterically hindered, C-substituted derivatives. For these latter bisadducts, it is reasonable to think that the relative yield of the *cis*-1 bisadducts would be lower than 1.4%.

In the attempt to shed light on some of the key factors responsible for the amplification in the formation of *M*/*P*-**1**(S_a,R_a), some control experiments were carried out, all of them involving some variation of the standard reaction (see Section 3). Firstly, a reaction was carried out replacing C_{60} fullerene by **3**, with the aim of identifying if this latter monoadduct could be a possible intermediate species in the formation of *M*/*P*-**1**(S_a,R_a). In this case, only unreacted **3** and newly formed **4** were recovered, with no sign of the formation of *M*/*P*-**1**(S_a,R_a). Next, a reaction was carried out in which the volume of toluene used was increased ten times (i.e., 150 mL, [**2**] = 0.3 mM) with respect to the standard reaction. In the case of the diluted reaction, *M*/*P*-**1**(S_a,R_a) was obtained in a 2% yield upon isolation, a value significantly lower than the 14% obtained in the standard reaction. In a third control experiment, DABCO was added to the reaction mixture (**2**/DABCO molar ratio = 2:1). In this latter case, the 14% yield of the isolated *M*/*P*-**1**(S_a,R_a), obtained under the standard reaction conditions fell to 4%. In the last control experiment, one reactant of the standard reaction (i.e., **2**) was replaced with the Zn^{II}Pc **6**, bearing six bulky 2,6-diphenylphenoxy substituents at the Pc periphery (Figure 1). In this case, a UV/Vis analysis of all the isolated species did not show the presence of any *H*-type Pc_2–C_{60} bisadduct.

From the outcome of the first control experiment, it can be inferred that **3** is not likely a key intermediate in the formation of *M*/*P*-**1**(S_a,R_a), thus suggesting that the two Pc addends are probably added simultaneously to the fullerene cage. The following two control experiments suggest that π-stacking interactions between **2** (or azomethyne ylide derivatives of **2**) must play a fundamental role in the formation of *M*/*P*-**1**(S_a,R_a), because when the concentration of these supramolecular Pc aggregates in solution was decreased, either by diluting the reaction or by the addition of DABCO, which hampers the Pc self-aggregation, the formation of *M*/*P*-**1**(S_a,R_a) was strongly reduced. The importance of Pc π-stacking interactions in the formation of *M*/*P*-**1**(S_a,R_a) was further confirmed in the last control experiment in which the use of a bulky Zn^{II}Pc derivative completely suppressed the formation of any Pc *H*-stacked C_{60} bisadduct.

Besides Pc π-stacking interactions, other noncovalent forces such as: 1) electrostatic interactions between the azomethyne ylide zwitterions (which could help stabilize the π-stacked Pc dimer maintaining the two pendant azomethyne ylide moieties in close proximity, ultimately favoring their *cis*-1 addition to the C_{60} cage; Table S6.6) and/or 2) attractive intramolecular London dispersion forces between the Pcs peripheral *tert*-butyl groups (which have been recently demonstrated to have a strong impact on the thermodynamic stability of molecules and on chemical reactions such as cycloadditions)[29] could also play an important role in the formation of *M*/*P*-**1**(S_a,R_a).

In conclusion, we have demonstrated that noncovalent interactions between untethered and prochiral residues bearing large π-surfaces can be successfully used, for the first time,

to promote the regio-, stereo-, and atropselective synthesis of C_{60} bisadducts. Although supramolecular interactions have been widely employed to construct complex architectures involving C_{60} fullerene,[30] their use as a tool to control and significantly amplify the formation of C_{60} bisadducts is unprecedented. We reckon that this supramolecular-directed approach represents an important conceptual and practical advance in the research area of the controlled multifunctionalization of fullerenes, which could be extended to other carbon nanoforms and molecular platforms.[31]

Acknowledgments

Financial support from the Spanish MINECO (CTQ2014-52869-P, CTQ2014-52774-P), the Comunidad de Madrid, Spain (FOTOCARBON, S2013/MIT-2841), the "Generalitat de Catalunya" (2014SGR-199 and XRQTC), and the European Union within the FP7-ENERGY-2012-1, Nr. 309194-2, GLOBASOL Project, is acknowledged.

Keywords: atropisomerism · cycloaddition · fullerenes · phthalocyanines · supramolecular chemistry

How to cite: *Angew. Chem. Int. Ed.* **2016**, *55*, 11020–11025
Angew. Chem. **2016**, *128*, 11186–11191

[1] R. K. M. Bouwer, J. C. Hummelen, *Chem. Eur. J.* **2010**, *16*, 11250 – 11253.
[2] Y. He, H.-Y. Chen, J. Hou, Y. Li, *J. Am. Chem. Soc.* **2010**, *132*, 1377 – 1382.
[3] S. Kitaura, K. Kurotobi, M. Sato, Y. Takano, T. Umeyama, H. Imahori, *Chem. Commun.* **2012**, *48*, 8550 – 8552.
[4] N. C. Miller, S. Sweetnam, E. T. Hoke, R. Gysel, C. E. Miller, J. A. Bartelt, X. Xie, M. F. Toney, M. D. McGehee, *Nano Lett.* **2012**, *12*, 1566 – 1570.
[5] Y. Matsuo, J. Kawai, H. Inada, T. Nakagawa, H. Ota, S. Otsubo, E. Nakamura, *Adv. Mater.* **2013**, *25*, 6266 – 6269.
[6] X. Meng, G. Zhao, Q. Xu, Z. Tan, Z. Zhang, L. Jiang, C. Shu, C. Wang, Y. Li, *Adv. Funct. Mater.* **2014**, *24*, 158 – 163.
[7] A. Hirsch, I. Lamparth, H. R. Karfunkel, *Angew. Chem. Int. Ed. Engl.* **1994**, *33*, 437 – 438; *Angew. Chem.* **1994**, *106*, 453 – 455.
[8] L. Isaacs, R. F. Haldimann, F. Diederich, *Angew. Chem. Int. Ed. Engl.* **1994**, *33*, 2339 – 2342; *Angew. Chem.* **1994**, *106*, 2434 – 2437.
[9] C. Thilgen, S. Sergeyev, F. Diederich, *Top. Curr. Chem.* **2005**, *248*, 1 – 61.
[10] M. Taki, S. Sugita, Y. Nakamura, E. Kasashima, E. Yashima, Y. Okamoto, J. Nishimura, *J. Am. Chem. Soc.* **1997**, *119*, 926 – 932.
[11] Y. Nakamura, A. Asami, T. Ogawa, S. Inokuma, J. Nishimura, *J. Am. Chem. Soc.* **2002**, *124*, 4329 – 4335.
[12] U. Reuther, T. Brandmuller, W. Donaubauer, F. Hampel, A. Hirsch, *Chem. Eur. J.* **2002**, *8*, 2261 – 2273.
[13] T. Hino, K. Saigo, *Chem. Commun.* **2003**, 402 – 403.
[14] R. Tao, T. Umeyama, T. Higashino, T. Koganezawa, H. Imahori, *ACS Appl. Mater. Interfaces* **2015**, *7*, 16676 – 16685.
[15] J.-F. Nierengarten, V. Gramlich, F. Cardullo, F. Diederich, *Angew. Chem. Int. Ed. Engl.* **1996**, *35*, 2101 – 2103; *Angew. Chem.* **1996**, *108*, 2242 – 2244.
[16] S. Sergeyev, F. Diederich, *Angew. Chem. Int. Ed.* **2004**, *43*, 1738 – 1740; *Angew. Chem.* **2004**, *116*, 1770 – 1773.
[17] N. Chronakis, A. Hirsch, *Chem. Commun.* **2005**, 3709 – 3711.
[18] T. Da Ros, M. Prato, V. Lucchini, *J. Org. Chem.* **2000**, *65*, 4289 – 4297.
[19] N. Martín, M. Altable, S. Filippone, A. Martin-Domenech, M. Guell, M. Sola, *Angew. Chem. Int. Ed.* **2006**, *45*, 1439 – 1442; *Angew. Chem.* **2006**, *118*, 1467 – 1470.
[20] M. R. Cerón, M. Izquierdo, A. Aghabali, J. A. Valdez, K. B. Ghiassi, M. M. Olmstead, A. L. Balch, F. Wudl, L. Echegoyen, *J. Am. Chem. Soc.* **2015**, *137*, 7502 – 7508.
[21] M. Prato, M. Maggini, *Acc. Chem. Res.* **1998**, *31*, 519 – 526.
[22] G. Bottari, D. Olea, C. Gomez-Navarro, F. Zamora, J. Gomez-Herrero, T. Torres, *Angew. Chem. Int. Ed.* **2008**, *47*, 2026 – 2031; *Angew. Chem.* **2008**, *120*, 2056 – 2061.
[23] A. W. Snow in *The Porphyrin Handbook*, *Vol. 17* (Eds.: K. M. Kadish, K. M. Smith, R. Guillard), Academic Press, San Diego, **2003**, pp. 129 – 176.
[24] O. Trukhina, M. Rudolf, G. Bottari, T. Akasaka, L. Echegoyen, T. Torres, D. M. Guldi, *J. Am. Chem. Soc.* **2015**, *137*, 12914 – 12922.
[25] L. Cecchi, F. De Sarlo, F. Machetti, *Eur. J. Org. Chem.* **2006**, 4852 – 4860.
[26] K. Kordatos, S. Bosi, T. Da Ros, A. Zambon, V. Lucchini, M. Prato, *J. Org. Chem.* **2001**, *66*, 2802 – 2808.
[27] T. Nishimura, K. Tsuchiya, S. Ohsawa, K. Maeda, E. Yashima, Y. Nakamura, J. Nishimura, *J. Am. Chem. Soc.* **2004**, *126*, 11711 – 11717.
[28] N. Marom, A. Tkatchenko, M. Scheffler, L. Kronik, *J. Chem. Theory Comput.* **2010**, *6*, 81 – 90.
[29] J. P. Wagner, P. R. Schreiner, *Angew. Chem. Int. Ed.* **2015**, *54*, 12274 – 12296; *Angew. Chem.* **2015**, *127*, 12446 – 12471.
[30] E. M. Pérez, N. Martin, *Chem. Soc. Rev.* **2008**, *37*, 1512 – 1519.
[31] T. Umeyama, J. Baek, Y. Sato, K. Suenaga, F. Abou-Chahine, N. V. Tkachenko, H. Lemmetyinen, H. Imahori, *Nat. Commun.* **2015**, *6*, 7732.

Received: March 18, 2016
Published online: May 9, 2016

